Nanoparticles

DOI: 10.1002/anie.201002557

Low-Symmetry Iron Oxide Nanocrystals Bound by High-Index Facets**

Jingzhou Yin, Zhinan Yu, Feng Gao, Jianjun Wang, Huan Pang, and Qingyi Lu**

Single crystals have a basic property of anisotropy and exhibit different physical and chemical properties on various facets or in diverse directions.[1–3] Generally, the properties of nanocrystals can be finely tuned, spanning a range of applications, by their shape to determine surface atomic arrangement and coordination.[4–7] The surface properties of materials highly depend on the shape of the nanocrystals and have great influence on the activity of nanocrystals in chemical reactions.[1] Thus, unprecedented research efforts have been focused on the controllable preparation of micro- and nanocrystals with various geometries and exposed surfaces. To date, most of the synthesized nanocrystals are enclosed by low-index {111} and {100} surfaces. Examples include tetrahedral,[8] octahedral,[9] decahedral,[10] and icosahedral[11] nanocrystals bound by {111} surfaces and nanocubes[12] enclosed by {100} surfaces to minimize surface energy.[2] Compared to the low-index facets, high-index facets usually have high surface energy and grow faster than the other facets, which makes them ultimately disappear during crystal growth.[3] However, also because of the high surface energy and the high density of atomic steps, ledges, and kinks of high-index facets, these facets can endow nanocrystals with high activity, thus promoting their potential applications as highly efficient catalysts and in special optical, electrical, and magnetic devices.[1,2] Accordingly, the synthesis of nanocrystals with exposed high-energy facets has become an important and challenging task. To date, there are just a few reports on the preparation of nanocrystals with exposed high-index facets. For example, Sun and co-workers first reported the synthesis of tetrahexahedral platinum nanocrystals in 2007.[1] Then the groups of Han and Kuang reported the syntheses of gold nanocrystals with high-index facets (such as {110}).[2,3] In 2009, Fang and co-workers reported the high-yield synthesis of elongated tetrahexahedral gold nanocrystals enclosed by 24 {037} facets.[13] The compounds in these reports about exposed high-index facets are metal elements with simple cubic crystal systems, and there are few reports on the synthesis of binary compounds with complex crystal systems, except the synthesis of GeO_2 and TiO_2 with high-energy facets.[14–16] However, compared with metal elements, binary compounds and compounds that do not crystallize in the cubic crystal system are more complex and have wider applications. The preparation of these kinds of compounds with high-index surfaces exposed would bring materials with high and special activities, thus facilitating their potential applications and expanding their application ranges.

Herein, we report for the first time two kinds of iron oxide crystals in the hexagonal crystal system: tetrakaidecahedra and oblique parallelepipeds with high-index facets exposed. The tetrakaidecahedral form has a three-fold axis bound by {012}, {102}, and {001} facets, while the oblique parallelepiped form looks like a cube but with one angle that is approximately 85° bound by {012}, {01−4}, and {−210} facets. Owing to the fact that iron oxide belongs to the hexagonal system, but not to the cubic system, these exposed high-index facets are very special, and the two kinds of brand-new polyhedra have never been reported before. Magnetic studies uncovered that these two forms of iron oxide have distinct differences. The tetrakaidecahedral iron oxide nanocrystals might be spin-canted ferromagnetically controlled at room temperature, and the ferromagnetism disappears at temperatures lower than T_m. The oblique parallelepiped nanocrystals might have coexistent spin-canted and defect ferromagnetism at room temperature and be defect ferromagnetically controlled at low temperature.

These two kinds of nanocrystals were obtained separately on a large scale through a simple reaction assisted by viscous macromolecules to adjust the reaction and growth rates. For the synthesis of tetrakaidecahedral iron oxide nanocrystals, a mixture of $K_3[Fe(CN)_6]$ (0.16 g), N_2H_4 solution (80%, 0.8 mL), and 2.8 g L^{-1} sodium carboxymethyl cellulose (CMC, 300–800 MPa S, 10 mL) solution was kept at 160 °C under solvothermal conditions for 6 h. Powder X-ray diffraction (XRD) confirms that the obtained product collected from the supernatant solution has hexagonal iron oxide structure (JCPDS 84-0311) with high purity and crystallinity (Figure 1 a). The Mössbauer spectrum (Figure S1a in the Supporting Information) of the sample at room temperature shows a single sextet and thus provides clear evidence for the presence of α-Fe_2O_3 rather than γ-Fe_2O_3 or Fe_3O_4.[17] Fig-

[*] J. Z. Yin, Prof. F. Gao, J. J. Wang
Department of Materials Science and Engineering
Nanjing University, Nanjing 210093 (China)
E-mail: fgao@nju.edu.cn
J. Z. Yin, Z. N. Yu, H. Pang, Prof. Q. Y. Lu
State Key Laboratory of Coordination Chemistry
Coordination Chemistry Institute
Nanjing National Laboratory of Microstructures
Nanjing University, Nanjing 210093 (China)
E-mail: qylu@nju.edu.cn
J. Z. Yin
School of Chemistry and Chemical Engineering
Huaiyin Normal University, Huai'an 223300 (China)

[**] This work was supported by the National Natural Science Foundation of China (Grant Nos. 50772047, 20671049, and 20721002), the National Basic Research Program of China (Grant No. 2007CB925102), and the Program for New Century Excellent Talents in University.

Supporting information for this article is available on the WWW under http://dx.doi.org/10.1002/anie.201002557.

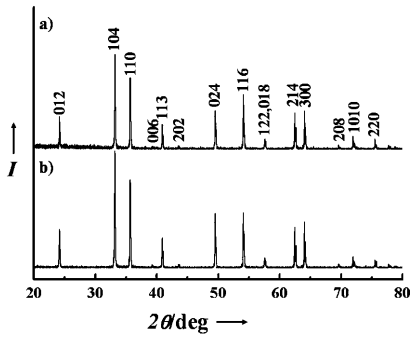

Figure 1. XRD patterns of a) the tetrakaidecahedral iron oxide nanocrystals and b) the oblique parallelepiped iron oxide nanocrystals.

ure 2a shows a typical large-area scanning electron microscope (SEM) image of the sample, indicating the presence of homogeneous, well-shaped nanocrystals with sizes ranging from 200 to 400 nm. As shown in high-magnification SEM images (Figure 2b,c), the as-prepared nanocrystals are well-shaped polyhedra comprising two top surfaces and twelve side surfaces and are, thus, tetrakaidecahedral. The two top surfaces are triangles with side lengths less than 100 nm. The cross-section in the middle of the crystal is an inequilateral hexagon with a trigonal axis. In other words, the tetrakaidecahedral crystals are bound by two top triangles, six side triangles, and six side trapezoids. This tetrakaidecahedron does not have a six-fold axis and is a shape rarely observed for nanocrystals. In Figure 2d, a geometrical model of an ideal tetrakaidecahedron enclosed by these crystal planes has been presented from side and top views, and it is in agreement with the as-prepared nanocrystals. The two top surfaces could be indexed to (001) and (00−1), respectively. The exposed side planes are (012), (102), (1−12), (0−12), (−102), (−112), and (01−2), (10−2), (1−1−2), (0−1−2), (−10−2), (−11−2). These results could be further confirmed by high-resolution transmission electron microscopy (HRTEM) images projected from the [241] direction. TEM images (Figure 2e,f) of the obtained sample display polyhedron-like structures with uniform size around 400 nm. The HRTEM image (Figure 2g) shows two groups of facets perpendicular to each other; their crystal plane spacings are 2.5 and 2.7 Å, which could be indexed to be (−210) and (01−4), respectively. Thus, this HRTEM image of the tetrakaidecahedron nanocrystals can be indexed to the [241] zone axis of a single iron oxide crystal. Similar results could be obtained from the SAED pattern shown in the inset of Figure 2g. These results not only suggest that the nanocrystals are single crystals, rather than multiply twinned crystals, but they also are in good agreement with the ideal tetrakaidecahedron model enclosed by {012} trapezoid-series facets, {102} triangle-series facets, and {001} top-series facets. Facets belonging to the same family usually have the same growth ratio; however, in the special tetrakaidecahedron, the facets in same family have been found to have two different growth ratios, which might open a door in crystal growth design. Also, it can be found that some of the surfaces of iron oxide crystals look rough. This phenomenon might be caused by the secondary growth of crystals in the basic solution.[18]

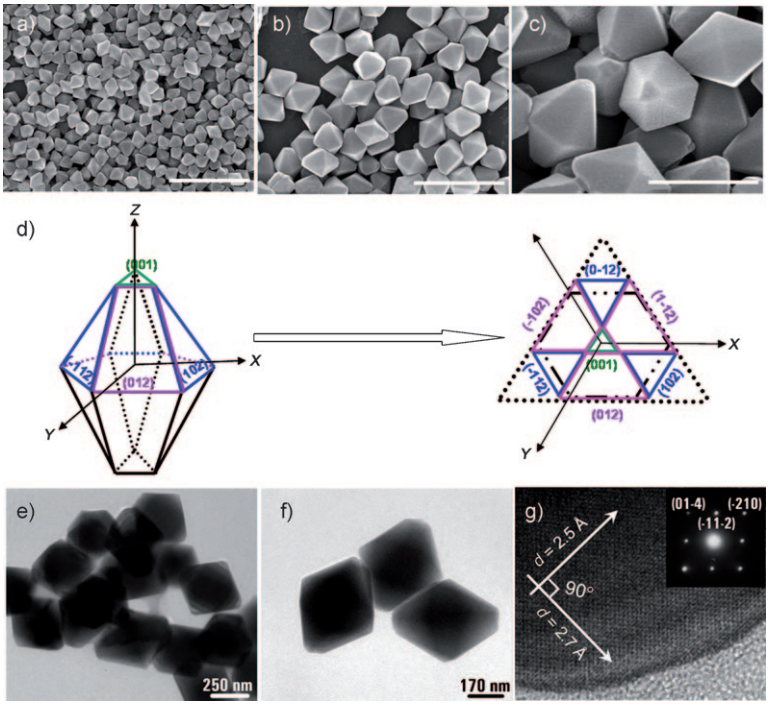

Figure 2. a–c) SEM images of the tetrakaidecahedral iron oxide nanocrystals. Scale bars: a) 2 μm, b) 1 μm, c) 500 nm. d) Side-view (left) and top-view (right) geometrical models of the tetrakaidecahedral iron oxide nanocrystals bound by {012}, {102}, and {001} facets. e,f) TEM images of the tetrakaidecahedral iron oxide nanocrystals. g) HRTEM image and SAED pattern (inset) of the tetrakaidecahedral iron oxide nanocrystals projected from the [241] direction.

For the synthesis of the other kind of iron oxide nanocrystals, a mixture of $K_3[Fe(CN)_6]$ (0.16 g), N_2H_4 solution (80%, 3 mL), and 2.8 g L^{-1} CMC solution (10 mL) was kept at 160 °C under solvothermal conditions for 6 h. The product collected from the supernatant solution is also confirmed to be hexagonal iron oxide by XRD (Figure 1b) and Mössbauer spectroscopy (Figure S1b in the Supporting Information). SEM investigations reveal that the majority of the sample is composed of quasi-cubic nanocrystals with an average edge length of 300 nm. Figure 3a shows a representative SEM image of the as-prepared product, indicating that the obtained sample has quasi-cubic shape. From the high-magnification SEM images shown in Figure 3b,c it could be seen that these quasi-cubes seem to be oblique parallelepipeds with one dihedral angel near 90° (ca. 85°), which means that the quasi-cubic crystal might not be enclosed by {001} as usual. According to the standard data of the hexagonal iron oxide crystal structure, (012) and (01−4) are perpendicular to (−210), and the dihedral angel between (012) and (01−4) is 85°, which is in quite good agreement with the above oblique parallelepiped. Thus, these nanocrystals might be bound by {012}, {01−4}, and {−210}.

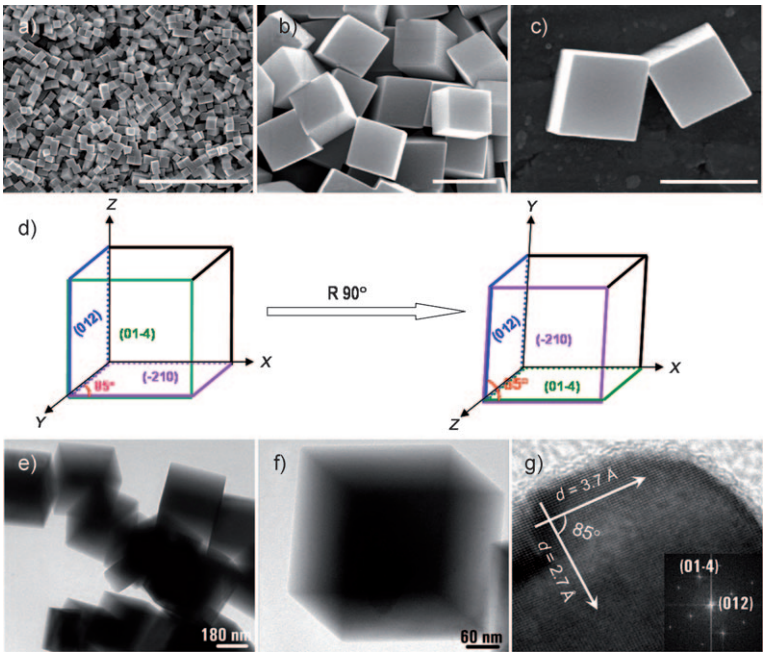

Figure 3. a–c) SEM images of the oblique parallelepiped iron oxide nanocrystals. Scale bars: a) 5 μm, b) 500 nm, c) 400 nm. d) Geometrical model of the oblique parallelepiped iron oxide nanocrystal bound by {012}, {01−4}, and {−210} facets. R = Rotation. e, f) TEM images of the oblique parallelepiped iron oxide nanocrystal. g) HRTEM image and FFT transformation pattern (inset) of the oblique parallelepiped iron oxide nanocrystals projected from the [100] direction.

Figure 3d presents a geometrical model of an ideal oblique parallelepiped enclosed by these facets in two different side views, which are in agreement with the as-prepared nanocrystals. Figure 3e–g show the sample's TEM images and the HRTEM image and its FFT transformation. The TEM images also confirm that the obtained sample has oblique parallelepiped shape with edge length of about 300 nm. The HRTEM image of an oblique parallelepiped nanocrystal shows two groups of facets which are at 85° and have crystal plane spacings of 3.7 and 2.7 Å, corresponding to be (012) and (01−4) planes, respectively. Thus, the HRTEM image of the oblique parallelepiped nanocrystal is projected from the [100] zone axis of a single crystal of hexagonal iron oxide. Similar results could be obtained from its FFT transformation. These results suggest that the nanocrystals are single crystals bound by {012}, {01−4}, and {−210}, in a good agreement with SEM results and the ideal oblique parallelepiped model.

In our experiments, the tetrakaidecahedral and the oblique parallelepiped nanocrystals could be synthesized separately, both in high yields. These two kinds of crystals could be obtained on a large scale by a very simple reaction in the presence of sodium carboxymethyl cellulose and the addition of N_2H_4. Without the addition of N_2H_4 and CMC, when aqueous $K_3[Fe(CN)_6]$ was treated under hydrothermal conditions at 160 °C for 6 h, α-Fe_2O_3 micropine dendrites were obtained with a size of several micrometers (Figure S2 in the Supporting Information), which is the result of the weak dissociation of $[Fe(CN)_6]^{3-}$ ions under hydrothermal conditions and the fast growth along six crystallographically equivalent directions of α-Fe_2O_3. A detailed study of the dendritic micropine Fe_2O_3 was also reported.[19] The morphology of α-Fe_2O_3 can be dramatically changed in the presence of CMC. When $K_3[Fe(CN)_6]$ in aqueous CMC was hydrothermal treated at 160 °C for 6 h but without the addition of N_2H_4, the obtained Fe_2O_3 nanoparticles are cubic-like with a size of about 80 nm, much smaller than the size of the micropine dendrites. As known, the CMC molecules have many carboxymethyl side groups, which prevents CMC backbones from getting close to each other.[20] So the solution can be divided into numerous "channels" by the CMC molecules in the reaction system to confine the growth of α-Fe_2O_3 nanoparticles, thus leading to the formation of Fe_2O_3 nanoparticles with much smaller size. With the addition of N_2H_4, the basic environment would make the Fe_2O_3 nanoparticles grow faster. The different adsorption properties of the different planes of Fe_2O_3 would lead to the formation of Fe_2O_3 polyhedra with different exposed surfaces.[21] For the synthesis of tetrakaidecahedral iron oxide nanocrystals, 0.8 mL N_2H_4 solution (80%) was used, while for the synthesis of the other kind of iron oxide nanocrystals, 3 mL N_2H_4 solution (80%) was used. The amount of N_2H_4 determines the final form of the crystals. As the amount of N_2H_4 is gradually changed from 0.8 to 3 mL, the morphology of the iron oxide nanocrystals transforms from pure terakaidecahedron to pure oblique parallelepiped. Figure S3a–c in the Supporting Information shows the SEM images of the products with different amounts of N_2H_4. With 1.0 mL N_2H_4, the morphology of the products is almost tetrakaidecahedral, and very few oblique parallelepiped particles can be seen in Figure S3a. As the amount of N_2H_4 increases, the percentage of tetrakaidecahedral Fe_2O_3 particles decreases, while that of the oblique parallelepiped particles increases (Figure S3b,c). The amount of N_2H_4 can influence the pH value of the solution. For comparison, we also used $NH_3{\cdot}H_2O$ as additive rather than N_2H_4, but only particles with spherical morphology can be obtained (see SEM images in Figure S4 in the Supporting Information). From these results, the addition of N_2H_4 and CMC is the key factor in the formation of the terakaidecahedral and oblique parallelepiped iron oxide nanocrystals with exposed high-indexed surfaces.

Hexagonal iron oxide is an important magnetic material, and it would be of great interest to investigate the magnetic properties of two α-Fe_2O_3 nanocrystals with different shapes and different exposed high-index facets. α-Fe_2O_3 is antiferromagnetic below T_N (955 K);[22] intrinsic (spin-canted) ferromagnetism and defect ferromagnetism occur in α-Fe_2O_3, and it shows weak ferromagnetic properties at room temperature.[23] The magnetic phase transition from the spin-canted ferromagnetic phase to the antiferromagnetically ordered state has been reported to be at approximately 260 K, which leads to a sharp decrease in magnetization, called the Morin transition temperature (T_m).[24] Unlike intrinsic spin-canted

ferromagnetism, the defect ferromagnetism is sensitive to structure and is altered by stress or heating and suppresses the Morin transition.[23] Figure 4a–c shows the magnetization-temperature curves (field-cooled under 100 Oe (FC) and zero-field-cooled (ZFC)) of tetrakaidecahedral iron oxide nanocrystals and the corresponding hysteresis loops at 300 and 50 K. The *M*–*T* curves display a decrease at a temperature of approximately 230 K, corresponding to Morin transition. This value is lower than the T_m of the bulk iron oxide samples because of the size and shape dependence of T_m.[19] The noticeable hysteresis at 300 K clearly shows that tetrakaidecahedral iron oxide nanocrystals are in a weak ferromagnetic state with a coercive field of approximately 300 Oe. At the lower temperature of 50 K the hysteresis loop disappears and the sample reveals an antiferromagnetic state, which corresponds to the Morin transition. This result indicates that the tetrakaidecahedral iron oxide nanocrystals might be spin-canted ferromagnetically controlled, and the ferromagnetism disappears at temperatures lower than T_m. However, the magnetic behaviors of oblique parallelepiped nanocrystals are different. As shown in Figure 4d–f, the magnetization-temperature curves just show a slight decrease near 230 K, corresponding to T_m. The sample shows another decrease at temperature of approximately 120 K. With further decrease of the temperature, the oblique parallelepiped nanocrystals still show weak ferromagnetic properties, which is different from the bulk iron oxide materials and the tetrakaidecahedral iron oxide nanocrystals. Correspondingly, the noticeable hysteresis at 300 K clearly shows that oblique parallelepiped nanocrystals are in a weak ferromagnetic state with a coercive field of about 400 Oe. The hysteresis loop measured at 50 K shrinks but still exists, unlike that of tetrakaidecahedra. This finding means that the oblique parallelepiped sample is weakly ferromagnetic at low temperature, in agreement with the *M*–*T* curves. These results show that although the transition from spin-canted ferromagnetism to antiferromagnetism is also observed in oblique parallelepiped nanocrystals, it is not the controlled phase transition in the sample. The oblique parallelepiped nanocrystals still show weak ferromagnetism under T_m, which means a long-range magnetic ordering still exists at low temperature. Similar phenomena have been recently observed in α-Fe_2O_3 nanotubes, for which the origin of the magnetic phase transition was attributed to the defects in nanotubes coming from the curl of layers.[25] In our case, the oblique parallelepiped nanocrystals are surrounded by high-indexed crystal faces having high surface energy and might show defect-controlled ferromagnetism because of the structure-sensitivity of defect ferromagnetism.[23] Although to reach a clear conclusion requires further investigations, the oblique parallelepiped nanocrystals might show coexistent spin-canted and defect ferromagnetism at room temperature and be defect ferromagnetically controlled at low temperature.

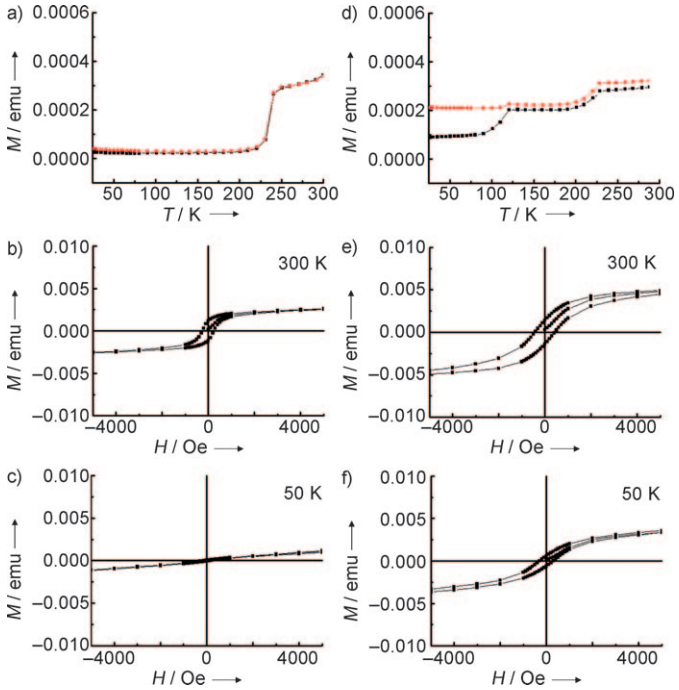

Figure 4. a) ZFC/FC (at 100 Oe, black ZFC, red FC) and b, c) magnetization (*M*) versus magnetic field (*H*) at 300 and 50 K of the tetrakaidecahedral iron oxide nanocrystals. d) ZFC/FC (at 100 Oe, black ZFC, red FC) and e, f) Magnetization (*M*) versus magnetic field (*H*) at 300 and 50 K of the oblique parallelepiped iron oxide nanocrystals.

In summary, unusual tetrakaidecahedral and oblique parallelepiped iron oxide nanocrystals with exposed high-index facets have been successfully synthesized in high yields with the assistance of the viscous macromolecule sodium carboxymethyl cellulose. The tetrakaidecahedral crystals have a three-fold axis bound by two top surfaces ((001) and (00−1)) and twelve side surfaces, including six triangles ((102), (0−12), (−112), (10−2), (0−1−2), (−11−2)) and six trapezoids ((012), (1−12), (−102), (0−12), (1−1−2), (−10−2)). The oblique parallelepiped crystals have two-fold axes enclosed by {012}, {01−4}, and {−210} facets. Magnetic measurements confirm that these two kinds of nanocrystals display shape-dependent magnetic behaviors. The tetrakaidecahedral iron oxide nanocrystals might be spin-canted ferromagnetically controlled at room temperature, and the ferromagnetism disappears at temperatures lower than T_m. The oblique parallelepiped nanocrystals might show coexistent spin-canted and defect ferromagnetism at room temperature and be defect ferromagnetically controlled at low temperature. The proposed new and simple method could not only be developed for the syntheses of nanocrystals with various high-index facets exposed but also be beneficial to the exploration of materials with new properties.

Received: April 29, 2010
Published online: July 26, 2010

Keywords: carbohydrates · high-index facets · iron oxide · magnetic properties · nanoparticles

[1] N. Tian, Z. Y. Zhou, S. G. Sun, Y. Ding, Z. L. Wang, *Science* **2007**, *316*, 732.

[2] G. H. Jeong, M. Kim, Y. W. Lee, W. Choi, W. T. Oh, Q. H. Park, S. W. Han, *J. Am. Chem. Soc.* **2009**, *131*, 1672.
[3] Y. Y. Ma, Q. Kuang, Z. Y. Jiang, Z. X. Xie, R. B. Huang, L. S. Zheng, *Angew. Chem.* **2008**, *120*, 9033; *Angew. Chem. Int. Ed.* **2008**, *47*, 8901.
[4] J. Zhang, K. Sasaki, E. Sutter, R. R. Adzic, *Science* **2007**, *315*, 220.
[5] V. R. Stamenkovic, B. Fowler, B. S. Mun, G. F. Wang, P. N. Ross, C. A. Lucas, N. M. Marković, *Science* **2007**, *315*, 493.
[6] R. Narayanan, M. A. El-Sayed, *Nano Lett.* **2004**, *4*, 1343.
[7] F. J. Vidal-Iglesias, J. Solla-Gullon, P. Rodríguez, E. Herrero, V. Montiel, J. M. Feliu, A. Aldaz, *Electrochem. Commun.* **2004**, *6*, 1080.
[8] F. Kim, S. Connor, H. Song, T. Kuykendall, P. D. Yang, *Angew. Chem.* **2004**, *116*, 3759; *Angew. Chem. Int. Ed.* **2004**, *43*, 3673.
[9] C. C. Li, K. L. Shuford, Q. H. Park, W. P. Cai, Y. Li, E. J. Lee, S. O. Cho, *Angew. Chem.* **2007**, *119*, 3328; *Angew. Chem. Int. Ed.* **2007**, *46*, 3264.
[10] A. Sánchez-Iglesias, I. Pastoriza-Santos, J. Pérez-Juste, B. Rodríguez-González, F. J. García de Abajo, L. M. Liz-Marzán, *Adv. Mater.* **2006**, *18*, 2529.
[11] K. Kwon, K. Y. Lee, Y. W. Lee, M. Kim, J. Heo, S. J. Ahn, S. W. Han, *J. Phys. Chem. C* **2007**, *111*, 1161.
[12] Y. G. Sun, Y. N. Xia, *Science* **2002**, *298*, 2176.
[13] T. Ming, W. Feng, Q. Tang, F. Wang, L. D. Sun, J. F. Wang, C. H. Yan, *J. Am. Chem. Soc.* **2009**, *131*, 16350.
[14] P. Liu, C. X. Wang, X. Y. Chen, G. W. Yang, *J. Phys. Chem. C* **2008**, *112*, 13450.
[15] H. G. Yang, C. H. Sun, S. Z. Qiao, J. Zou, G. Liu1, S. C. Smith, H. M. Cheng, G. Q. Lu, *Nature* **2008**, *453*, 638.
[16] B. H. Wu, C. Y. Guo, N. F. Zheng, Z. X. Xie, G. D. Stucky, *J. Am. Chem. Soc.* **2008**, *130*, 17563.
[17] R. M. Cornell, U. Schwertmann, *The Iron Oxides*, VCH, Weinheim, **1996**.
[18] J. Z. Yin, Q. Y. Lu, Z. N. Yu, J. J. Wang, H. Pang, F. Gao, *Cryst. Growth Des.* **2010**, *10*, 40.
[19] M. H. Cao, T. F. Liu, S. Gao, G. B. Sun, X. L. Wu, C. W. Hu, Z. L. Wang, *Angew. Chem.* **2005**, *117*, 4269; *Angew. Chem. Int. Ed.* **2005**, *44*, 4197.
[20] http://class.fst.ohio-state.edu/fst621/Additive%20classes/ggum3.pdf.
[21] C. J. Murphy, *Science* **2002**, *298*, 2139.
[22] F. Grønvold, E. J. Samuelsen, *J. Phys. Chem. Solids* **1975**, *36*, 249.
[23] D. J. Dunlop, *Science* **1970**, *169*, 858.
[24] F. Morin, *Phys. Rev.* **1950**, *78*, 819.
[25] L. Liu, H. Z. Kou, W. L. Mo, H. J. Liu, Y. Q. Wang, *J. Phys. Chem. B* **2006**, *110*, 15218.

